# Long-term retention of ECM hydrogel after implantation into a sub-acute stroke cavity reduces lesion volume

Harmanvir Ghuman, B.S.[1,2], Madeline Gerwig[3], Francesca J. Nicholls, Ph.D.[1,4], Jessie Liu[2], Julia Donnelly[5], Stephen F. Badylak, DVM, PhD, M.D.[1,2,6], and Michel Modo, Ph.D.[1,2,4,*]

[1]McGowan Institute for Regenerative Medicine, University of Pittsburgh

[2]Department of Bioengineering, Pittsburgh, Pennsylvania, USA

[3]Department of Neuroscience, Pittsburgh, Pennsylvania, USA

[4]Department of Radiology, Pittsburgh, Pennsylvania, USA

[5]Department of Biological Sciences, Pittsburgh, Pennsylvania, USA

[6]Department of Surgery, Pittsburgh, Pennsylvania, USA
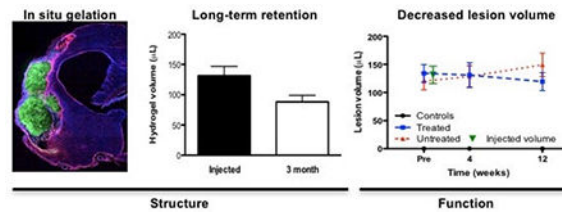
## Abstract

Salvaging or functional replacement of damaged tissue caused by stroke in the brain remains a major therapeutic challenge. In situ gelation and retention of a hydrogel bioscaffold composed of 8 mg/mL extracellular matrix (ECM) can induce a robust invasion of cells within 24 hours and potentially promote a structural remodeling to replace lost tissue. Herein, we demonstrate a long-term retention of ECM hydrogel within the lesion cavity. A decrease of approximately 32% of ECM volume is observed over 12 weeks. Lesion volume, as measured by magnetic resonance imaging and histology, was reduced by 28%, but a battery of behavioral tests (bilateral asymmetry test; footfault; rotameter) did not reveal a therapeutic or detrimental effect of the hydrogel. Glial scarring and peri-infarct astrocytosis were equivalent between untreated and treated animals, potentially indicating that permeation into host tissue is required to exert therapeutic effects. These results reveal a marked difference of biodegradation of ECM hydrogel in the stroke-damaged brain compared to peripheral soft tissue repair. Further exploration of these structure-function relationships is required to achieve a structural remodeling of the implanted hydrogel, as seen in peripheral tissues, to replace lost tissue and promote behavioral recovery.

## Graphical abstract

---

*Corresponding Author: Dr. Mike Modo, University of Pittsburgh, McGowan Institute for Regenerative Medicine, 3025 East Carson St, Pittsburgh, PA 15203, USA, +1 (412) 383 7200, modomm@upmc.edu.

## Keywords

Extracellular matrix; Magnetic resonance imaging; Stroke; Hydrogel; Behavior; Tissue Repair; Biodegradation; Biomaterial; Implantation; Cell Invasion

## 1. Introduction

Extracellular matrix (ECM) is a complex collection of molecules produced by cells that serve structural and functional roles. The ECM creates an interface between cells to provide structural support and mechanical strength to tissue, but also exerts juxtacrine signaling, resulting in functional effects on constituent cells [1]. The decellularization of tissues affords the reformulation of ECM as a bioscaffold that conveys structural, as well as functional properties in aiding and enhancing soft tissue repair [2]. ECM can be derived from a variety of tissue sources (e.g. urinary bladder, skin, CNS) [3] and has found translation into a clinical setting to repair urinary bladder, muscle, peripheral nerve and heart, as well as being used in breast reconstruction [4-8].

Bioscaffolds composed of ECM consistently promote a pro-repair host inflammatory response that contributes to functional remodeling outcomes in many anatomic sites. ECM hydrogels consist of solubilized and repolymerized ECM and contain signaling molecules that can influence cell differentiation [9]. In contrast, synthetic scaffolds, such as polyethylene glyocol (PEG) hydrogels, typically require functionalization to achieve similar repair properties [10, 11]. Implantation of ECM typically induces a constructive structural remodeling of the bioscaffold mediated by the invasion of cells, notably macrophages, and subsequent deposition of site appropriate tissue [3]. Through degradation of the ECM bioscaffold and the release of signaling molecules, macrophages can be activated toward a repair phenotype promoting a gradual host tissue cell invasion, including stem/progenitor cells [12]. Invasion of tissue-specific cells leads to a replacement of the scaffold to reconstitute a functional tissue [13]. Biodegradation studies reveal that this process is fairly rapid, with approximately half of the material being remodeled within 30 days and a complete replacement being noted between 75-90 days post-implantation in several peripheral tissue locations [14-18]. The ECM bioscaffold provides the substrate for cell invasion, but the degradation of the scaffold is an essential process for the release of additional signaling molecules, positioning of host-derived stem cells and the deposition of new matrix derived from host-organ cells [9, 19]. The biodegradation process of bioscaffolds can also be exploited to deliver therapeutic factors to the peri-infarct area to influence host remodeling or the inflammatory response. Although there is consistency across different

peripheral soft tissues in this process [3], at present it is unclear if the same principle is recapitulated in the damaged central nervous system, specifically the stroke-damaged brain.

In vitro comparisons of ECM pre-gel derived from porcine brain, spinal cord, optic nerve and urinary bladder (UBM) indicated that all preparations were cytocompatible and stimulated proliferation, migration, as well as differentiation and neurite outgrowth of neural progenitors [20, 21]. Of these, UBM-ECM produced the highest neurite outgrowth in PC12 cells [21], as well as cell migration of perivascular stem cells [20], especially at high concentrations (>10 μg/mL). The rheological properties of UBM-ECM are similar to brain-ECM, but significantly lower to the 5× stiffer spinal cord ECM [22]. Brain and spinal cord ECM are therefore potential candidates for CNS tissue repair, but the widely-used UBM-ECM provides favorable characteristics to induce a structural remodeling response.

UBM-ECM hydrogel also provides an excellent survival and differentiation of neural stem cells (NSCs) after transplantation into animals with traumatic brain injury [23]. A combination of UBM-ECM with 10% brain-ECM also resulted in the survival of NSCs implanted into stroke cavity, with evidence of some host invasion into hydrogel void of NSCs [24]. To exploit this cell invasion and harness endogenous tissue repair, ECM needs to form a stable hydrogel within the stroke cavity. UBM-ECM requires a concentration of >3mg/mL to form a hydrogel that is retained within the cavity, revealing a structure-function relationship that is governed in part by the rheological properties of the ECM preparation [25]. Concentrations >3 mg/mL exhibit a significant invasion of host cells, predominantly monocytes (i.e. macrophages/microglia) that are activated towards an M2-repair phenotype [26], consistent with the process of biodegradation observed in other organs. The most significant cell invasion, monocyte activation and recruitment of neural progenitors were evident at 8 mg/mL [26], suggesting that a high content of soluble components increased the recruitment of appropriate cells [12]. This significant acute recruitment of host cells into the ECM scaffold suggests that the structural formulation of the material leads to an acute cellular response that is akin to peripheral soft tissues [3].

In addition to promoting a host repair response that could lead to the reconstitution of brain tissue, implantation of a bioscaffold after stroke can also provide structural support to the host brain avoiding tissue deformation (e.g. midline shift, ventricular enlargement), as well as local delivery of growth factors, neural stem cells, and other medicinal products. However, little is known about the long-term interaction between host tissue and biomaterial in the stroke-damaged brain. The extent of stroke damage continues to evolve over time with further tissue loss [27]. Limiting the progression of this long-term tissue loss could hence stabilize the stroke environment and provide a more fertile ground for other therapeutic interventions, such as stem cell therapy [19, 28, 29].

To determine the long-term structure-function relationship of ECM hydrogel and peri-infarct host tissue, we investigated an ECM preparation (8 mg/mL) that is retained inside the stroke cavity to provide structural support [25, 30], but also provides a strong signaling environment to recruit large numbers of host cells that can promote structural remodeling of the material [26]. The objective of the present study was to evaluate if this hydrogel formulation of ECM (i.e. structure) undergoes biodegradation inside a stroke cavity, akin to

peripheral soft tissues, and if its continued presence or remodeling affects host tissue deformation, as well behavioral impairments after a stroke (i.e. function).

## 2. Methods

### 2.1. Extracellular matrix (ECM) hydrogel

To produce an ECM hydrogel, the basement membrane and tunica propria of adult porcine urinary bladder (Tissue Source, Inc., Lafayette, IN) were isolated by mechanical delamination, as previously described [31]. Decellularization was performed using 0.1% peracetic acid in 4% ethanol (v/v; 120 min; 300 rpm) with agitation. A series of PBS and deionized water rinses removed cellular debris. Decellularization was confirmed using Hematoxylin & Eosin, 4′,6-diamidino-2-phenylindole (DAPI) staining, agarose gel electrophoresis, and quantification of remnant DNA [2]. The remaining ECM was lyophilized, comminuted, and solubilized with pepsin (1 mg/mL) in 0.01 N HCl. pH neutralization was achieved by adding 0.1 N NaOH. Approximately 70% of the overall material is collagen [22], but other prominent ECM proteins, such as fibronectin, decorin, laminin subunit $\gamma$1 are also present [32]. A variety of growth factors are also retained within the ECM preparation, including transforming growth factor-$\beta$, vascular endothelial growth factor-A, basic fibroblast growth factor, and nerve growth factor [21], which all are known to influence neuronal and endothelial cells. In addition, matrix-bound nanovesicles (MBV) enriched in miRNA and other signaling molecules are present within the ECM preparation [33].

Dilution to a desired concentration (8 mg/mL) was attained by suspension in the appropriate volume of PBS [31]. Gelation of this preparation is concentration, pH and temperature-dependent. Concentrations <3 mg/mL do not readily form a hydrogel [25, 26]. An 8 mg/mL preparation achieves a viscosity of 0.443 Pa * s, takes 3 min to reach 50% gelation with a maximum storage modulus (G') of 460.4 Pa, which exceeded its loss modulus of 66.4 Pa. This preparation approximated the reported 500-1000 Pa elastic modulus of brain tissue [34-36].

### 2.2. Middle Cerebral Artery Occlusion (MCAo)

All animal procedures complied with the US Animals Welfare Act (2010) and were approved by the University of Pittsburgh Institutional Animal Care and Use Committee (IACUC). Sprague-Dawley rats (male, 260±15g, Taconic Labs, USA) were maintained on a 12-hour light/dark schedule, with food and water available *ad libitum.* Animals were randomly assigned (using a random number sequence) to either undergo MCAo or serve as a control. For transient intraluminal right middle cerebral artery (MCA) occlusion, a rat model of stroke, a 5-0 silicone rubber-coated monofilament (diameter 0.12 mm, length 30 mm, tip coating at 0.35 mm for 5-6 mm, 503556PK10, Doccol, USA) was advanced to the ostium of the MCA in the circle of Willis under isoflurane (4% induction, 1% maintenance in 30% $O_2$) anesthesia. The MCA was occluded for 70 minutes prior to reperfusion by retracting the filament to the common carotid bifurcation. After recovery from anesthesia, animals were assessed for forelimb flexion and contralateral circling with daily post-operative care and neurological assessment until they recovered pre-operative weight [37, 38]. Animals not

exhibiting signs of MCA damage or who failed to recover weight were excluded at this stage (Figure 1A). Control animals received a neck incision to maintain blinding of researchers based on external markings.

## 2.3. Magnetic Resonance Imaging (MRI)

**Acquisition**—To assess the presence, location and volume of tissue loss, MCAo rats were anesthetized with isoflurane (4% induction, 1% maintenance) and scanned using a $T_2$-weighted spin-echo MRI sequence (TR = 6000 ms, TE = 8 ms, 8 Averages, FOV 30x30 mm, 128x128 matrix, 42 slices at 0.5 mm thickness) on a horizontal bore 9.4 T Varian scanner 10 days post-infarction [30].

**Lesion volume and intensity measurements**—Stroke damage was defined as tissue with a hyperintense signal on $T_2$-weighted images that were thresholded at 1 standard deviation above the mean of a rectangular region of interest (ROI) in the contralateral hemisphere, encompassing striatum, corpus callosum and neocortex [39, 40]. Rats (n=22) with lesion volume >40 mm$^3$ (i.e. 40 μL) were randomly assigned to either the untreated or the ECM treated group (Figure 1A), resulting in an equivalent distribution of lesion volumes across both groups. Lesion volumes ranged from 72-246 μL. Reporting of random group allocation, as well as exclusion/inclusion of animals (Figure 1A), complies with the principles set forth to ensure transparency in preclinical research [41, 42].

**Tissue deformation measurements**—ROIs were defined based on anatomical characteristics to segment host tissue and determine if ECM implantation affected the deformation of the brain due to stroke damage. A midline shift is commonly observed due to the host tissue expanding with the void of the lesion cavity not providing sufficient structural support. Midline shift was determined by placing a vertical line from the longitudinal fissure to the median eminence at Bregma +0.7, which commonly is the central slice of MCAo damage. In the middle of the vertical line, perpendicular lines are drawn to measure the distance to the edge of each hemisphere. A ratio is taken of these two measurements to define the relative midline shift. Ventricular enlargement is also often seen as a consequence of tissue deformations. Volume changes of tissue parenchyma were also calculated to determine if stroke and ECM implantation affected structural changes in these regions.

## 2.4. Implantation procedure

Fourteen days post-stroke (Figure 1B), rats underwent ECM implantation by placement into a stereotactic frame (Kopf, USA) under isoflurane anesthesia (4% induction, 1% maintenance in 30% $O_2$). A vertical skin incision exposed Bregma on the skull and provided guidance for the location of Burr holes for the placement of a 250 μL Hamilton syringe with a 24 G beveled tip metal needle (Hamilton) filled with solubilized 8 mg/mL ECM in PBS, as well as a hole for a drainage cannula (24 G) [25]. Ideally, a needle with a very small bore size is used for injection of biomaterials to minimize injection damage to intact or damaged brain tissue [43]. Nevertheless, the potential aggregation and gelation of biomaterials can clog the needle and hence a large needle size (24G) is required to ensure the efficient delivery of material, as well as minimize damage to brain tissue [44]. MR images of lesion location and volumes were used to define stereotactic coordinates for needle/cannula

placements [25, 43]. Needles/cannula were slowly lowered into brain tissue. Lesion-equivalent volumes of solubilized ECM (72-246 μL) were injected into the ventral posterior region of the cavity to displace and drain the less dense necrotic debris from the most dorsal part of the lesion [25]. We have previously demonstrated that a precise neurosurgical planning is required for these large volume injections to avoid misplacement or leaching of material into the lateral ventricles, but also to avoid damage to structures in the path of injection [25, 30]. Injection of ECM hydrogel (n=11) was controlled using a frame mounted injection pump (World Precision Instruments, USA) at a constant speed of 10 μL/min until the total volume was delivered (7-25 min). The solubilized ECM formed a hydrogel in situ at 37 °C body temperature. Needle and cannula were left in place for 5 minutes to allow material to dissipate and gel before the needles were slowly withdrawn from the brain. Burr holes were filled with bone wax (Fisher) prior to suturing. Untreated and control animals received the same head incisions without burr hole drilling to maintain blinding of researchers based on visible markings. LX4 (Ferndale, containing 4% Lidocaine) was topically applied as an analgesic, as well as buprenorphine (0.5 mg/kg) i.p. to provide sustained pain relief.

## 2.5. Behavioral Assessment

Establishing the efficacy of ECM hydrogel injection to recover behavioral deficits in an animal model of stroke requires evaluation of these deficits on a variety of tests that reflect damage to sensorimotor, motor, and cognitive systems (Figure 1B). Researchers blinded to the condition of animals performed all acquisition of data, graphing and statistical analyses. Animals from different groups were mixed in cages.

**Bilateral Asymmetry Test—**The bilateral asymmetry test probed tactile extinction as a measure of sensory neglect [28, 37, 38]. For this, two strips of equal size (6 cm long, 0.5-0.8 cm wide) were applied with equal pressure to the saphenous part of the forepaw. Four trials (180 seconds each) recorded the time to contact and removal for each paw. Sensorimotor bias was determined by subtracting the unaffected (right) from the affected (left) paw.

**Footfault Test—**The footfault test evaluated the animals' ability to integrate motor responses by analyzing motor impairments of limb functioning and placing deficits during locomotion [28, 37, 38]. The rats were placed in the Motorater System (TSE GmbH) with horizontal bars to record the placements of both unaffected and affected forelimbs over 8 trials (>60 placements). A comparison of total number of incorrect placements or % missed steps across groups measured performance on motor integration.

**Rotameter—**Amphetamine-induced rotations (2.5 mg/kg in saline, i.p.) were measured using an automated rotameter system (TSE Systems). Rotational bias is used as an index of striatal damage [28, 37]. Animals were harnessed into jackets tethered to the rotameter system and injected with amphetamine 30 minutes prior to assessment. Contralateral and ipsilateral rotations were recorded for 30 minutes.

### 2.6. Histological analyses

**Perfusion-fixation of tissue—**To analyze the distribution of the ECM hydrogel and cell infiltration within the hydrogel, rats were transcardially perfused at 90 days post-implantation with 0.9% saline followed by 4% paraformaldehyde (in 0.2 M PBS) to fix brain tissue prior to its removal from the skull. Brains were post-fixed in 4% paraformaldehyde for 24 hours prior to being cryopreserved in 30% sucrose with sodium azide (Sigma) at 4 °C . Histological sections (50 μm thickness) were cut on a cryostat (Leica) directly onto microscopic slides.

**Immunohistochemistry—**Brain sections were washed 3x5 minutes with 0.01 M PBS, followed by 1 hr permeabilization in PBS + 0.1% Triton X-100 (Sigma) at room temperature (21 °C). Primary antibodies (Table 1) were then applied, diluted in PBS + 0.05% Triton X-100, and incubated at 4 °C overnight. After rinsing of the primary antibodies (3x5 min PBS), appropriate secondary AlexaFluor 488, 555, or 660 antibodies (1:500; Life Technologies) were applied for 1 hour at room temperature followed by 3x5 min washed with PBS. Finally, sections were coverslipped with Vectashield for fluorescence containing Hoechst 33342 (1 μg/mL, Sigma) and stored at 4 °C prior to imaging. Visualization of antibodies was performed with a fluorescence microscope (Axioimager M2, Zeiss) interfaced with a monochrome camera driven by Stereo Investigator image capture software (MBF Bioscience) using a motorized stage.

**ECM hydrogel volume—**The virtual tissue module tiled individual 10× images into whole hemisphere images. In order to determine the total volume of the injected ECM present at the final time point (Day 90), anterior-posterior whole biomaterial images (500 μm apart) were acquired to measure the area occupied by ECM (i.e. collagen I staining), and then multiplied by the distance between images to approximate total scaffold volume.

**Parenchyma and lesion volume—**To compare the amount of parenchymal volume, freehand ROIs were drawn around the tissue for each hemisphere, including the ventricles, on 8-bit whole brain histology images in Fiji version 1.49 (https://fiji.sc). Volumes for the left and right lateral ventricles were also measured and subtracted from corresponding hemispheres to account for differences in ventricular size to yield parenchymal volume for each hemisphere. A ratio between ipsi- and contralateral parenchymal and ventricular volumes was calculated for comparison. Due to tissue loss in the stroke hemisphere, the volume of the contralateral hemisphere served as reference value to calculate lesion volume by subtracting ipsilateral parenchymal volume from the contralateral parenchymal volume (both excluding ventricular volume). Total lesion volume was calculated by multiplying the area measurement by the distance to the next slice (500 μm).

**Scarring measurements—**Brain tissue sections were stained with GFAP before acquiring whole brain images at 10× magnification. Images were acquired with 100 ms exposure time for all animals to provide a consistent signal intensity across all sections. The images were then processed through Fiji to define straight lines as ROIs starting from the lesion boundary and drawing away from the cavity. An intensity vs. distance plot was then

created to determine the thickness of the glial scar in both cortex and striatum. These ROIs were drawn in all anterior-posterior brain sections containing the glial scarring.

**Peri-infarct astrocytosis**—In order to determine the percent area covered by astrocytes in both ipsilateral (i.e. right) stroke-affected and contralateral (i.e. left) unaffected hemispheres, whole brain GFAP stained images were first converted to 8-bit images before applying a threshold to mask GFAP+ cells and create a binary map. The same threshold value was used for all brain sections to maintain consistency. ROIs were then drawn around both hemispheres (excluding the cavity and lateral ventricles) to determine the area fraction covered by astrocytes.

**Cell invasion**—To determine the number and phenotype of cells invading the injected ECM, collagen I was used to delineate the border between host and biomaterial. To quantify cell invasion, whole graft images were acquired at 20× magnification with brain sections stained for Hoechst (to identify cell nuclei) and Collagen I (to mask and delineate the host-ECM boundary) (Figure 2). Images were processed through Fiji to define grayscale images of the invading cells. Composite images of the biomaterial were untiled before quantifying the number of invading cells in Cell Profiler version 2.1.1 (http://cellprofiler.org).

**Cell Phenotypes**—For analysis of phenotypes of invading cells, images were acquired at 20× magnification to determine the total number of cells (i.e. Hoechst+) within the ECM material. 5-8 images were equally spaced throughout the material within a section and counted across all anterior-posterior slices containing ECM hydrogel. Phenotypic markers for neural progenitor cells (doublecortin, DCX), neurons (Fox3), astrocytes (glial fibrillary acid protein, GFAP), oligodendrocytes (2′,3′-cyclic-nucleotide 3′-phospodiesterase, CNPase), endothelial cells (rat endothelial cell antigen 1, RECA-1), microglia (ionized calcium-binding adapter molecule 1, Iba-1), as well as macrophage activation (CD206 for the M2 phenotype, CD86 for M1 phenotype) were used for analysis (Table 1). Although many mononuclear macrophages share histological markers, Iba-1 is a commonly used marker for brain microglia [45]. To account for differences in the number of invading cells, phenotypes were expressed as % of total cells present.

## 2.8. Statistical analyses

Statistical analyses were performed in SPSS 17 for Mac (IBM) with significance set at p<0.05. Specifically, a one-way ANOVA was used to compare cell invasion and phenotypes, using a Bonferroni post-hoc test to validate significant comparisons. A two-way ANOVA with Bonferroni post-hoc testing was used to contrast the comparison between lesion volumes, as well as behavioral data. Graphs were drawn in Prism 6 (GraphPad) with data points representing the mean and bars reflecting the standard deviation. A priori power calculations were performed in G*Power [46]. A power of 80% (Type II error) with a significance of p<0.05 (Type I error) is considered suitable [47]. With a medium effect size f of 0.25 for ANOVAs, a total sample size of N=36 is sufficient to achieve a power of 80% at the 5% significance level (Figure 1C).

# 3. Results

## 3.1. ECM implantation and evolution of lesion volume

The volume of implantation of ECM precursor was determined based on the hyperintense lesion volume, which was measured on pre-implantation $T_2$-weighted MR images (Figure 2A) using tissue segmentation (Figure 2B). After exclusion of animals with lesions <40 μL or no lesion, the remaining MCAo animals were randomly assigned to the untreated or treated MCAo groups, with both having equivalent mean lesion volumes of approximately 130 μL (Figure 2C). Untreated and treated animals' lesion volume was significantly different from controls (F=41.98, p<0.001), with treated rats showing a significant reduction in lesion volume at 12 weeks (p<0.05). By accounting for pre-implantation volume, untreated animals revealed a 28% increase in volume, whereas lesion volume in treated rats was significantly reduced (t=2.856, p<0.01) in comparison to untreated animals (Figure 2D). It is also noteworthy that there was a 10% decrease in volume compared to the 2 weeks post-infarct baseline volume, although this did not reach statistical significance. ECM implantation therefore attenuated the structural progression of stroke damage.

## 3.2. ECM and tissue deformation

To quantitatively determine the impact of ECM implantation on host tissue structures, pre-implantation and final MR images were further segmented. Hemispheric parenchymal volume was measured to determine if the reduction in lesion volume translated into novel brain tissue. However, there was no significant difference between treated and untreated animals (Figure 2E). This pattern of results was also evident for a midline shift (Figure 2F), right lateral ventricular volume (Figure 2G), and the ratio of left/right lateral ventricle (Figure 2H). The lack of host tissue changes therefore suggests that changes in $T_2$-weighted lesion volumes is a reflection of an attenuation of the tissue-lesion interface (i.e. T2 signal in lesion), rather than the generation of new tissue per se or a slowing ventricular enlargement.

## 3.3. ECM hydrogel does not impact behavioral functions

To determine the impact of ECM hydrogel on the brain, a battery of behavioral tests was employed to evaluate functional changes associated with different brain regions affected by stroke. Sensorimotor functions are dependent on striatal and sensorimotor cortex, both affected by stroke, and readily assessed by the bilateral asymmetry test (BAT). The contralateral hemisphere is unaffected by stroke and serves as an internal control. The right forepaw here was unaffected by stroke and was equivalent in all 3 experimental groups (Figure 3A). In contrast, the left affected forepaw exhibited a significant impairment in both untreated and treated MCAo animals compared to controls, with no evidence of ECM hydrogel altering this defect in a positive or negative fashion.

The footfault test is dependent on the motor loop of the striatum and motor cortex and demonstrates a robust long-term deficit after stroke. The right forepaw did not show any deficit walking over horizontal bars in any of the experimental groups (Figure 3B), whereas the left forepaw contralateral to the stroke lesion exhibited a significant impairment pre-implantation (p<0.001), with no indication of change due to ECM hydrogel evident at any time point.

In contrast to the BAT and footfault, the rotameter evaluates pharmacologically induced rotations that probe the hemispheric dopamine-balance in the striatum (Figure 3C), often considered a functional measure of the degree of striatal tissue loss. There was no bias in clockwise rotations between any of the experimental groups, but there was a significant bias in counterclockwise rotations in untreated and treated animals (p<0.001). No difference between untreated and treated animals was evident indicating that ECM hydrogel did not functionally affect host striatal tissue.

### 3.4. ECM hydrogel implantation decreases tissue cavitation

After completion of in vivo analyses, fixed tissue was processed for histological analyses. Stroke and the loss of brain tissue leads to the formation of a cavity that is delineated by a scar formed by glial cells, forming the edge of the tissue (Figure 4A). Implantation of 8 mg/mL ECM hydrogel into the cavity indicates that it is contained within the cavity delineated by gliosis. Although stroke significantly reduced the amount of parenchyma in the ipsilateral stroke hemisphere (F=67.58, p<0.001), the presence of ECM hydrogel in the lesion cavity did not significantly increase parenchymal volume in comparison to untreated animals (Figure 4B). There was also no evidence of a structural effect of ECM treatment on ventricular volume, although stroke significantly enlarged the ipsilateral ventricle in both groups relative to controls (F=3.41, p<0.05). A comparison of lesion volume between untreated and treated animals indicated that there was a 19.8% decrease in the cavity after ECM treatment (t=2.143, p<0.05).

### 3.5. Slow biodegradation produces long-term retention of ECM hydrogel

A macroscopic evaluation of the presence of ECM hydrogel revealed that the bioscaffold, as indicated by collagen I staining, was distributed throughout the lesion cavity (Figure 4C). Morphologically the ECM hydrogel appeared to reflect the pre-implantation MR lesion volume. Histological measurement of the ECM hydrogel volume along the anterior-posterior axis (Figure 4D) afforded a volumetric comparison of injected and retained ECM. There was a significant 32% decrease (t=6.737, p<0.001) in ECM hydrogel volume by 12 weeks post-implantation compared to the injected precursor volume (Figure 4E). Despite some biodegradation, a large amount of ECM hydrogel remains within the brain of all animals at 12 weeks post-implantation.

### 3.6. Glial scarring and peri-infarct astrocytosis are unaffected by ECM hydrogel

Using whole slice imaging of histological sections along the anterior-posterior axis allowed a quantitative determination of the extent of scarring in host tissue (Figure 4F). The extent of scarring was highest at the edge of the tissue and gradually declined. The intensity of the glial scar indicates a scar that is much more pronounced in the striatum than cortex. A comparison between untreated and treated animals revealed no significant difference in scarring in striatum or cortex (Figure 4G). Thresholding and quantification of the area of astrocytosis in the peri-infarct area (Figure 4H) also did not reveal a significant effect of ECM in the ipsi- or contralateral hemisphere (Figure 4I).

### 3.7. Presence of host cells is not correlated with injected and retained ECM volume

Host cells invaded the ECM hydrogel with cells scattered throughout the bioscaffold (Figure 5A). Quantification of cells within the hydrogel (Figure 5B) indicated some variability with a range of 44,820 to 78,740 cells (mean = 65,050) per animal. To investigate if this variability is associated with the volume of injected ECM, a correlation analysis between these was performed (Figure 5C), but did not reveal a strong significant correlation (r=0.33, n.s.). Lesion volume did also not predict (r=0.35, n.s.) the number of cells that were present within the ECM hydrogel (Figure 5D). Cells within the ECM hydrogel were clustered, rather than distributed in a homogenous distribution. In some cases, an organization along grooves was observed in the hydrogel (Figure 5E). In a few cases, the cellular organization consisted of endothelial cells forming tubules, but in most cases such cell accumulations consisted of other cell phenotypes.

### 3.8. Microglia and oligodendroctes predominantly invade ECM hydrogel

To assess the phenotypes of cells inside the ECM hydrogel, immunohistochemical markers for individual cell lineages (neural progenitors, neurons, astrocytes, oligodendrocytes, endothelial cells, and microglia) found in brain tissue were quantified (Figure 6A). The vast majority of cells within the ECM were of a microglia (Iba1, 51%) phenotype (F=130.6, p<0.001; Figure 6B), with fewer cells being oligodendrocytes (CNPase; 31%) and very few cells being endothelial (RECA1, 3.75) cells and astrocytes (GFAP, 1.3%). Neurons (Fox3, 4.2%) and neural progenitors (DCX, 0.15%) were rarely seen within the material at 90 days. A 36.4% co-expression of M1 (CD86)- and M2 (CD206)-like characteristics on monocytes (i.e. microglia/macrophages) was most commonly observed. Significantly fewer cells (F=20.27, p<0.001) presented with an exclusive M1 (9.5%)- or M2 (4.8%)-like phenotype (Figure 6C).

## 4. Discussion

The formation of a tissue cavity in the brain is commonly the result of a severe acute tissue injury, such as stroke [48] or traumatic brain injury (TBI) [49], but can also be caused by a surgical intervention to evacuate a hematoma [50], or the resection of a neoplasm [51]. The loss of tissue is associated with severe disability and structural deformations of host tissue leading to behavioral dysfunctions through Wallerian degeneration or tissue compacting [52]. As ECM hydrogel can be retained within this tissue cavity [25] and promote the infiltration of site-appropriate phenotypes [26], we here determined that an 8 mg/mL ECM hydrogel was retained long-term (12 weeks) after implantation with only moderate signs of biodegradation. The retention of some host cells that invaded was also evident. These cells were predominantly pro-repair microglia and oligodendrocytes that were sparsely distributed. There was a significant effect on lesion volume as determined by MRI, but there was no reduction in tissue deformation caused by the stroke. No effect on a battery of behavioral tests was evident, indicating minimal impact on host tissue function. These results therefore indicate that an 8 mg/mL ECM concentration promoted a reduction in lesion volume, but did not undergo a rapid biodegradation as observed in peripheral soft tissue that could support extensive tissue repair.

## Biodegradation of ECM bioscaffold in brain

ECM bioscaffolds typically undergo a 50% biodegradation within 30 days and are fully degraded between 75-90 days in volumetric soft tissue defects [18]. Bioscaffolds are often considered to provide the 'soil' to seed stem cells from the host organ [19]. Implantation of ECM into the stroke-damaged brain induces a very significant infiltration of host cells within 24 hours, akin to that observed in peripheral organs [26]. This initiation of a constructive remodeling response is essential for tissue repair [9] and is governed by a principle of dynamic reciprocity in which the ECM adapts to the structural, mechanical and functional needs of cells [53]. Although there was a 32% decrease in ECM volume over 12 weeks here, the significant retention of the hydrogel within the tissue cavity indicates that biodegradation of this material in the brain is slower than that in peripheral soft tissue.

Structural elements, such as pore size and fiber orientation, within the ECM hydrogel can influence the biodegradation properties of a scaffold [54]. ECM hydrogels with a denser fiber architecture typically show a slower biodegradation, as evidenced by dermal ECM hydrogel taking longer to degrade than an equivalent concentration of UBM-ECM [55]. Fiber diameter ($0.7 \ \mu m$), pore size ($0.10 \ \mu m^2$), and node density (6 nodes/$\mu m^2$) are well conserved between 2 and 8 mg/mL UBM-ECM concentrations [55]. Pore sizes within these preparations are smaller than NSCs, which we established to have a diameter of ~20 μm [44]. A significant invasion of NSCs was nevertheless observed within 1 day post-implantation suggesting that migration itself was not hindered [26]. Smaller pore size in gelatin scaffolds (50-200 μm) are thought to induce differentiation of chondrocytes, whereas larger pores (250-500 μm) support proliferation [56], potentially indicating that invading NSCs differentiate rather than migrate into the scaffold. Still, little is known about how porosity influences neural stem cell migration and differentiation. It is important to note that cells can change their shape to migrate through smaller pores and pore size can also be enlarged by macrophages pushing apart or degrading fibers [57]. Although pore size provides a geometry that facilitates cell migration, with larger pore size increasing cell migration [56, 58], soluble factors also influence cell behavior by diffusing through these pores [12].

Macrophage infiltration and their activation toward a M2-phenotype have been implicated in ECM remodeling [59] and been identified as a key process for tissue replacement [3, 13]. Cells contained within the matrix here were predominantly macrophages and microglia with a M2-polarization indicating that the scaffold maintained an appropriate biodegradation response. However, there were very few cells present here at 12 weeks (mean=65,050 cells) compared to those reported at 1 day (mean=366,278cells) post-implantation [26]. This difference of 82% fewer cells potentially explains the lack of or extremely slow degradation response. It remains unclear why the number of cells within the material would decrease so dramatically after 1 day. A time course study investigating the cellular infiltration and degradation response of different ECM concentrations will be required to further address these issues.

The central nervous system is known to be an immune-privileged environment that has limited potential for self-repair [60]. Nevertheless, the host brain response to ECM hydrogel implantation suggests that the bioscaffold can attract significant numbers of host cells to

promote structural remodeling by 24 hours [26]. At 12 weeks, oligodendrocytes and microglia/macrophages were the dominant cell phenotypes with very few astrocytes, neural progenitors and neurons present. Still, the presence of neurons within the hydrogel is encouraging. The lack of neovascularization of the bioscaffold through endothelial cell invasion and organization is potentially a major factor impeding the structural remodeling of the implanted material. It remains unclear why revascularization of ECM hydrogel occurs efficiently in peripheral organs, but not in the brain. Improving the neovascularization of the scaffold could hence be a key factor to promote the degradation response and sustain invading brain cells.

**Structural support to host brain prevents lesion volume increase**

In addition to the release of biochemical factors from the ECM, its rheological properties are also likely to influence cell invasion and phenotypic differentiation. It is known that stiffer material tends to promote astrocytic, rather than neuronal, differentiation [61, 62]. Lower concentration hydrogels that are less stiff could hence undergo a more significant biodegradation and promote invasion of appropriate phenotypes to form a neurovascular environment. The slow biodegradation also maintains a stiffer environment, potentially limiting further cell invasion [63], as well as morphological cell changes required to align and form a novel vascular structure. Mechanosensing of hydrogels by host tissue also influences the interface with host tissue by creating a glia scar [64]. Nevertheless, cells infiltrated the material upon implantation through the scar. This suggest that neither the stiffness of the material, nor the dense gliosis at the edge of the tissue defect provided a barrier to cell invasion. There was no evidence here that ECM hydrogel impacted the extent of scarring or peri-infarct astrocytosis, further indicating a minimal impact on existing brain tissue.

As the hydrogel maintained its macroscopic structure within the cavity, it can also exert structural support to host brain tissue. The impact of stroke on the host brain is severe with a major loss of tissue leading to ventricular enlargement, progressive atrophy of the ipsilateral parenchyma and an enlargement of the contralateral hemisphere. These tissue deformations are reflected in a midline shift [27, 65], with pressure gradients within tissues producing secondary Wallerian degeneration of axonal connections and poorer outcomes [66, 67]. Reducing tissue deformation is considered beneficial to overall long-term deficits associated with infarction [52, 68]. A slowly degrading bioscaffold implanted into the stroke cavity could exert a supportive function for host tissue. Sufficient stiffness of the hydrogel will be required to ensure a structural support to surrounding tissue. Although there was minimal attenuation of ventricular enlargement and midline shift, a significant reduction in lesion volume compared to baseline and an ~40% difference to the untreated animals revealed structural effects of the hydrogel on the lesion environment. This difference in treated and untreated animals is likely a combination of the cumulative effects of smaller changes in parenchymal volume and right lateral ventricle. A more acute implantation of hydrogel in combination with the controlled local delivery of therapeutic compounds could provide new treatment approaches in stroke, traumatic brain injury and gliomas [69-72].

### ECM hydrogel does not affect behavioral function

ECM implantation has been reported to promote behavioral improvements in animal models of TBI [23, 73, 74]. However, in these cases smaller volumes at lower concentrations of ECM were injected without retention of material within the tissue cavity. We here demonstrated that the retention of urinary bladder ECM within the stroke cavity did not impact behavioral functions. No improvement in deficits was evident, but there was also no indication that the injection led to any deleterious effects. Long-term retention of ECM hydrogel therefore is likely to be safe for physical support and delivery of therapeutic factors, but a concentration of 8 mg/mL is not providing a therapeutic behavioral benefit by itself. It is hence possible that lower concentrations of ECM, which partially gel after injection, would permeate into surrounding tissue to produce beneficial therapeutic effects.

The interface and permeation of ECM into this area might be an important factor in achieving therapeutic efficacy. The implantation of human neural stem cells into the peri-infarct, for instance, has significantly improved the same behavioral deficits as assessed here within a 3 months' time frame [28] and might indicate that repair of pre-infarct tissue is a key process in achieving behavioral recovery. As lower concentrations (3-4 mg/mL) of ECM hydrogel permeate into this peri-infarct tissue [25], these concentrations might provide more favorable conditions to affect behavioral deficits [73], even though these preparations do not yield as significant a cell invasion after 24 hours of implantation [26]. In this case, the signaling properties of ECM hydrogel would induce the repair of damaged tissue, rather than necessitating a structural scaffold to support the invasion of cells to form a de novo tissue. Although collagen I is the most abundant molecules in UBM- ECM hydrogel and is likely to convey its rheological properties, it also contains a myriad of other proteins, oligopeptides, glycosaminoglycans, proteoglycans, growth factors and other juxtracine/paracrine signaling molecules (including nanovesicles). All of these can influence the repair response by modifying macrophage phenotype, stem cell recruitment and mechanotransduction. However, the variety and complexity of these molecules and their interaction in the damaged brain pose a harrowing challenge to elucidate a specific mechanism of repair. Further exploration of these extensive structure-function relationships is required to achieve a therapeutic efficacy comparable to the implantation of neural stem cells in the peri-infarct area, but also promoting conditions that improve the structural remodeling of ECM inside the lesion cavity to encourage the replacement of lost tissue, as seen in peripheral organs.

## 5. Conclusions

The tissue loss after a stroke constitutes a major challenge to improve behavioral outcomes. Implantation of a bioscaffold into the cavity can potentially provide physical support to the remaining host brain tissue, but inductive biomaterials can also attract host cells to invade. We here demonstrated that an 8 mg/mL concentration of UBM-ECM hydrogel can reduce the lesion cavity with minimal impact on host tissue, peri-infarct astrocytosis and glial scarring. The hydrogel was retained within the cavity for 12 weeks suggesting that the biodegradation of the material within the brain does not replicate the typical time course observed in peripheral tissues. Behavioral functions were not affected by the implantation or

Author Manuscript

retention of the material within the cavity indicating that an 8 mg/mL preparation appears safe for the local delivery of therapeutic factors, but by itself does not appear to exert a therapeutic benefit in stroke. Further studies are required using lower concentrations of ECM hydrogel that would afford permeation into the peri-infarct areas and potentially sustain a host response that could reproduce the structural remodeling observed in peripheral organs.

## Acknowledgments

## References

1. Marcoli M, Agnati LF, Benedetti F, Genedani S, Guidolin D, Ferraro L, Maura G, Fuxe K. On the role of the extracellular space on the holistic behavior of the brain. Rev Neurosci. 2015; 26(5):489–506. [PubMed: 26103627]

2. Crapo PM, Gilbert TW, Badylak SF. An overview of tissue and whole organ decellularization processes. Biomaterials. 2011; 32(12):3233–43. [PubMed: 21296410]

3. Aamodt JM, Grainger DW. Extracellular matrix-based biomaterial scaffolds and the host response. Biomaterials. 2016; 86:68–82. [PubMed: 26890039]

4. Badylak SF, Kochupura PV, Cohen IS, Doronin SV, Saltman AE, Gilbert TW, Kelly DJ, Ignotz RA, Gaudette GR. The use of extracellular matrix as an inductive scaffold for the partial replacement of functional myocardium. Cell Transplant. 2006; 15(1):S29–40. [PubMed: 16826793]

5. Fallon A, Goodchild T, Wang R, Matheny RG. Remodeling of extracellular matrix patch used for carotid artery repair. The Journal of surgical research. 2012; 175(1):e25–34. [PubMed: 22316677]

6. Sreejit P, Verma RS. Natural ECM as biomaterial for scaffold based cardiac regeneration using adult bone marrow derived stem cells. Stem cell reviews. 2013; 9(2):158–71. [PubMed: 23319217]

7. Kajbafzadeh AM, Payabvash S, Salmasi AH, Sadeghi Z, Elmi A, Vejdani K, Tavangar SM, Tajik P, Mahjoub F. Time-dependent neovasculogenesis and regeneration of different bladder wall components in the bladder acellular matrix graft in rats. The Journal of surgical research. 2007; 139(2):189–202. [PubMed: 17292410]

8. Pashos NC, Scarritt ME, Eagle ZR, Gimble JM, Chaffin AE, Bunnell BA. Characterization of an Acellular Scaffold for a Tissue Engineering Approach to the Nipple-Areolar Complex Reconstruction. Cells Tissues Organs. 2017; 203(3):183–193. [PubMed: 28125805]

9. Swinehart IT, Badylak SF. Extracellular matrix bioscaffolds in tissue remodeling and morphogenesis. Dev Dyn. 2016; 245(3):351–60. [PubMed: 26699796]

10. Zhu J, Marchant RE. Design properties of hydrogel tissue-engineering scaffolds. Expert Rev Med Devices. 2011; 8(5):607–26. [PubMed: 22026626]

11. Chan BP, Leong KW. Scaffolding in tissue engineering: general approaches and tissue-specific considerations. Eur Spine J. 2008; 17(4):467–79. [PubMed: 19005702]

12. Slivka PF, Dearth CL, Keane TJ, Meng FW, Medberry CJ, Riggio RT, Reing JE, Badylak SF. Fractionation of an ECM hydrogel into structural and soluble components reveals distinctive roles in regulating macrophage behavior. Biomater Sci. 2014; 2(10):1521–34. [PubMed: 26829566]

13. Brown BN, Badylak SF. Extracellular matrix as an inductive scaffold for functional tissue reconstruction. Transl Res. 2014; 163(4):268–85. [PubMed: 24291155]

14. Dearth CL, Slivka PF, Stewart SA, Keane TJ, Tay JK, Londono R, Goh Q, Pizza FX, Badylak SF. Inhibition of COX1/2 alters the host response and reduces ECM scaffold mediated constructive tissue remodeling in a rodent model of skeletal muscle injury. Acta Biomater. 2016; 31:50–60. [PubMed: 26612417]

15. Valentin JE, Stewart-Akers AM, Gilbert TW, Badylak SF. Macrophage participation in the degradation and remodeling of extracellular matrix scaffolds. Tissue Eng Part A. 2009; 15(7):1687–94. [PubMed: 19125644]

16. Gilbert TW, Stewart-Akers AM, Badylak SF. A quantitative method for evaluating the degradation of biologic scaffold materials. Biomaterials. 2007; 28(2):147–50. [PubMed: 16949150]

17. Carey LE, Dearth CL, Johnson SA, Londono R, Medberry CJ, Daly KA, Badylak SF. In vivo degradation of 14C-labeled porcine dermis biologic scaffold. Biomaterials. 2014; 35(29):8297–304. [PubMed: 24997479]

18. Record RD, Hillegonds D, Simmons C, Tullius R, Rickey FA, Elmore D, Badylak SF. In vivo degradation of 14C-labeled small intestinal submucosa (SIS) when used for urinary bladder repair. Biomaterials. 2001; 22(19):2653–9. [PubMed: 11519785]

19. Forbes SJ, Rosenthal N. Preparing the ground for tissue regeneration: from mechanism to therapy. Nat Med. 2014; 20(8):857–69. [PubMed: 25100531]

20. Crapo PM, Tottey S, Slivka PF, Badylak SF. Effects of biologic scaffolds on human stem cells and implications for CNS tissue engineering. Tissue Eng Part A. 2014; 20(1-2):313–23. [PubMed: 24004192]

21. Crapo PM, Medberry CJ, Reing JE, Tottey S, van der Merwe Y, Jones KE, Badylak SF. Biologic scaffolds composed of central nervous system extracellular matrix. Biomaterials. 2012; 33(13): 3539–47. [PubMed: 22341938]

22. Medberry CJ, Crapo PM, Siu BF, Carruthers CA, Wolf MT, Nagarkar SP, Agrawal V, Jones KE, Kelly J, Johnson SA, Velankar SS, Watkins SC, Modo M, Badylak SF. Hydrogels derived from central nervous system extracellular matrix. Biomaterials. 2013; 34(4):1033–40. [PubMed: 23158935]

23. Wang JY, Liou AK, Ren ZH, Zhang L, Brown BN, Cui XT, Badylak SF, Cai YN, Guan YQ, Leak RK, Chen J, Ji X, Chen L. Neurorestorative effect of urinary bladder matrix-mediated neural stem cell transplantation following traumatic brain injury in rats. CNS Neurol Disord Drug Targets. 2013; 12(3):413–25. [PubMed: 23469853]

24. Bible E, Dell'Acqua F, Solanky B, Balducci A, Crapo PM, Badylak SF, Ahrens ET, Modo M. Non-invasive imaging of transplanted human neural stem cells and ECM scaffold remodeling in the stroke-damaged rat brain by (19)F- and diffusion-MRI. Biomaterials. 2012; 33(10):2858–71. [PubMed: 22244696]

25. Massensini AR, Ghuman H, Saldin LT, Medberry CJ, Keane TJ, Nicholls FJ, Velankar SS, Badylak SF, Modo M. Concentration-dependent rheological properties of ECM hydrogel for intracerebral delivery to a stroke cavity. Acta Biomater. 2015; 27:116–30. [PubMed: 26318805]

26. Ghuman H, Massensini AR, Donnelly J, Kim SM, Medberry CJ, Badylak SF, Modo M. ECM hydrogel for the treatment of stroke: Characterization of the host cell infiltrate. Biomaterials. 2016; 91:166–81. [PubMed: 27031811]

27. Modo M, Beech JS, Meade TJ, Williams SC, Price J. A chronic 1 year assessment of MRI contrast agent-labelled neural stem cell transplants in stroke. Neuroimage. 2009; 47(2):T133–42. [PubMed: 18634886]

28. Smith EJ, Stroemer RP, Gorenkova N, Nakajima M, Crum WR, Tang E, Stevanato L, Sinden JD, Modo M. Implantation site and lesion topology determine efficacy of a human neural stem cell line in a rat model of chronic stroke. Stem Cells. 2012; 30(4):785–96. [PubMed: 22213183]

29. Boisserand LS, Kodama T, Papassin J, Auzely R, Moisan A, Rome C, Detante O. Biomaterial Applications in Cell-Based Therapy in Experimental Stroke. Stem Cells Int. 2016; 2016:6810562. [PubMed: 27274738]

30. Jin T, Nicholls FJ, Crum WR, Ghuman H, Badylak SF, Modo M. Diamagnetic chemical exchange saturation transfer (diaCEST) affords magnetic resonance imaging of extracellular matrix hydrogel implantation in a rat model of stroke. Biomaterials. 2017; 113:176–190. [PubMed: 27816001]

31. Freytes DO, Martin J, Velankar SS, Lee AS, Badylak SF. Preparation and rheological characterization of a gel form of the porcine urinary bladder matrix. Biomaterials. 2008; 29(11): 1630–7. [PubMed: 18201760]

32. Marcal H, Ahmed T, Badylak SF, Tottey S, Foster LJ. A comprehensive protein expression profile of extracellular matrix biomaterial derived from porcine urinary bladder. Regen Med. 2012; 7(2): 159–66. [PubMed: 22397606]

33. Huleihel L, Hussey GS, Naranjo JD, Zhang L, Dziki JL, Turner NJ, Stolz DB, Badylak SF. Matrix-bound nanovesicles within ECM bioscaffolds. Sci Adv. 2016; 2(6):e1600502. [PubMed: 27386584]

34. Taylor Z, Miller K. Reassessment of brain elasticity for analysis of biomechanisms of hydrocephalus. J Biomech. 2004; 37(8):1263–9. [PubMed: 15212932]

35. Aurand ER, Wagner J, Lanning C, Bjugstad KB. Building biocompatible hydrogels for tissue engineering of the brain and spinal cord. J Funct Biomater. 2012; 3(4):839–63. [PubMed: 24955749]

36. Gefen A, Margulies SS. Are in vivo and in situ brain tissues mechanically similar? J Biomech. 2004; 37(9):1339–52. [PubMed: 15275841]

37. Modo M, Stroemer RP, Tang E, Veizovic T, Sowniski P, Hodges H. Neurological sequelae and long-term behavioural assessment of rats with transient middle cerebral artery occlusion. J Neurosci Methods. 2000; 104(1):99–109. [PubMed: 11163416]

38. Modo M. Long-term survival and serial assessment of stroke damage and recovery - practical and methodological considerations. J Exp Stroke Transl Med. 2009; 2(2):52–68. [PubMed: 22389748]

39. Stille M, Smith EJ, Crum WR, Modo M. 3D reconstruction of 2D fluorescence histology images and registration with in vivo MR images: Application in a rodent stroke model. J Neurosci Methods. 2013; 219(1):27–40. [PubMed: 23816399]

40. Ashioti M, Beech JS, Lowe AS, Hesselink MB, Modo M, Williams SC. Multi-modal characterisation of the neocortical clip model of focal cerebral ischaemia by MRI, behaviour and immunohistochemistry. Brain research. 2007; 1145:177–89. [PubMed: 17320839]

41. Landis SC, Amara SG, Asadullah K, Austin CP, Blumenstein R, Bradley EW, Crystal RG, Darnell RB, Ferrante RJ, Fillit H, Finkelstein R, Fisher M, Gendelman HE, Golub RM, Goudreau JL, Gross RA, Gubitz AK, Hesterlee SE, Howells DW, Huguenard J, Kelner K, Koroshetz W, Krainc D, Lazic SE, Levine MS, Macleod MR, McCall JM, Moxley RT 3rd, Narasimhan K, Noble LJ, Perrin S, Porter JD, Steward O, Unger E, Utz U, Silberberg SD. A call for transparent reporting to optimize the predictive value of preclinical research. Nature. 2012; 490(7419):187–91. [PubMed: 23060188]

42. Macleod MR, Fisher M, O'Collins V, Sena ES, Dirnagl U, Bath PM, Buchan A, van der Worp HB, Traystman R, Minematsu K, Donnan GA, Howells DW. Good laboratory practice: preventing introduction of bias at the bench. Stroke. 2009; 40(3):e50–2. [PubMed: 18703798]

43. Bible E, Chau DY, Alexander MR, Price J, Shakesheff KM, Modo M. Attachment of stem cells to scaffold particles for intra-cerebral transplantation. Nature protocols. 2009; 4(10):1440–53. [PubMed: 19798079]

44. Rossetti T, Nicholls F, Modo M. Intra-cerebral cell implantation: Preparation and characterization of cell suspensions. Cell Transplant. 2015

45. Ito D, Tanaka K, Suzuki S, Dembo T, Fukuuchi Y. Enhanced expression of Iba1, ionized calcium-binding adapter molecule 1, after transient focal cerebral ischemia in rat brain. Stroke. 2001; 32(5):1208–15. [PubMed: 11340235]

46. Faul F, Erdfelder E, Buchner A, Lang AG. Statistical power analyses using G*Power 3.1: tests for correlation and regression analyses. Behav Res Methods. 2009; 41(4):1149–60. [PubMed: 19897823]

47. Lakens D. Calculating and reporting effect sizes to facilitate cumulative science: a practical primer for t-tests and ANOVAs. Front Psychol. 2013; 4:863. [PubMed: 24324449]

48. Moreau F, Patel S, Lauzon ML, McCreary CR, Goyal M, Frayne R, Demchuk AM, Coutts SB, Smith EE. Cavitation after acute symptomatic lacunar stroke depends on time, location, and MRI sequence. Stroke. 2012; 43(7):1837–42. [PubMed: 22733793]

49. Lee B, Newberg A. Neuroimaging in traumatic brain imaging. NeuroRx. 2005; 2(2):372–83. [PubMed: 15897957]

50. Vespa P, Hanley D, Betz J, Hoffer A, Engh J, Carter R, Nakaji P, Ogilvy C, Jallo J, Selman W, Bistran-Hall A, Lane K, McBee N, Saver J, Thompson RE, Martin N, Investigators I. ICES (Intraoperative Stereotactic Computed Tomography-Guided Endoscopic Surgery) for Brain Hemorrhage: A Multicenter Randomized Controlled Trial. Stroke. 2016; 47(11):2749–2755. [PubMed: 27758940]

51. Bette S, Gempt J, Huber T, Delbridge C, Meyer B, Zimmer C, Kirschke JS, Boeckh-Behrens T. FLAIR signal increase of the fluid within the resection cavity after glioma surgery: generally valid as early recurrence marker? J Neurosurg. 2016:1–9.

52. Breteler MM, van Amerongen NM, van Swieten JC, Claus JJ, Grobbee DE, van Gijn J, Hofman A, van Harskamp F. Cognitive correlates of ventricular enlargement and cerebral white matter lesions on magnetic resonance imaging. The Rotterdam Study, Stroke. 1994; 25(6):1109–15. [PubMed: 8202966]

53. Bissell MJ, Aggeler J. Dynamic reciprocity: how do extracellular matrix and hormones direct gene expression? Prog Clin Biol Res. 1987; 249:251–62. [PubMed: 3671428]

54. Loh QL, Choong C. Three-dimensional scaffolds for tissue engineering applications: role of porosity and pore size. Tissue Eng Part B Rev. 2013; 19(6):485–502. [PubMed: 23672709]

55. Wolf MT, Daly KA, Brennan-Pierce EP, Johnson SA, Carruthers CA, D'Amore A, Nagarkar SP, Velankar SS, Badylak SF. A hydrogel derived from decellularized dermal extracellular matrix. Biomaterials. 2012; 33(29):7028–38. [PubMed: 22789723]

56. Lien SM, Ko LY, Huang TJ. Effect of pore size on ECM secretion and cell growth in gelatin scaffold for articular cartilage tissue engineering. Acta Biomater. 2009; 5(2):670–9. [PubMed: 18951858]

57. Ciano PS, Colvin RB, Dvorak AM, McDonagh J, Dvorak HF. Macrophage migration in fibrin gel matrices. Lab Invest. 1986; 54(1):62–70. [PubMed: 3941542]

58. Wolf K, Te Lindert M, Krause M, Alexander S, Te Riet J, Willis AL, Hoffman RM, Figdor CG, Weiss SJ, Friedl P. Physical limits of cell migration: control by ECM space and nuclear deformation and tuning by proteolysis and traction force. J Cell Biol. 2013; 201(7):1069–84. [PubMed: 23798731]

59. Brown BN, Londono R, Tottey S, Zhang L, Kukla KA, Wolf MT, Daly KA, Reing JE, Badylak SF. Macrophage phenotype as a predictor of constructive remodeling following the implantation of biologically derived surgical mesh materials. Acta Biomater. 2012; 8(3):978–87. [PubMed: 22166681]

60. Bechmann I. Failed central nervous system regeneration: a downside of immune privilege? Neuromolecular Med. 2005; 7(3):217–28. [PubMed: 16247182]

61. Aurand ER, Lampe KJ, Bjugstad KB. Defining and designing polymers and hydrogels for neural tissue engineering. Neurosci Res. 2012; 72(3):199–213. [PubMed: 22192467]

62. Banerjee A, Arha M, Choudhary S, Ashton RS, Bhatia SR, Schaffer DV, Kane RS. The influence of hydrogel modulus on the proliferation and differentiation of encapsulated neural stem cells. Biomaterials. 2009; 30(27):4695–9. [PubMed: 19539367]

63. Ahearne M. Introduction to cell-hydrogel mechanosensing. Interface Focus. 2014; 4(2):20130038. [PubMed: 24748951]

64. Blakney AK, Swartzlander MD, Bryant SJ. The effects of substrate stiffness on the in vitro activation of macrophages and in vivo host response to poly(ethylene glycol)-based hydrogels. J Biomed Mater Res A. 2012; 100(6):1375–86. [PubMed: 22407522]

65. Soon HW, Qiu A. Individualized diffeomorphic mapping of brains with large cortical infarcts. Magn Reson Imaging. 2015; 33(1):110–23. [PubMed: 25278293]

66. Goldsmith W. The state of head injury biomechanics: past, present, and future: part 1. Crit Rev Biomed Eng. 2001; 29(5-6):441–600. [PubMed: 12434929]

67. Qiu W, Jiang Q, Xiao G, Wang W, Shen H. Changes in intracranial pressure gradients between the cerebral hemispheres in patients with intracerebral hematomas in one cerebral hemisphere. BMC Anesthesiol. 2014; 14:112. [PubMed: 25506260]

68. Jeon SB, Kwon SU, Park JC, Lee DH, Yun SC, Kim YJ, Ahn JS, Kwun BD, Kang DW, Choi HA, Lee K, Kim JS. Reduction of Midline Shift Following Decompressive Hemicraniectomy for Malignant Middle Cerebral Artery Infarction. J Stroke. 2016; 18(3):328–336. [PubMed: 27733025]

69. Tao J, Zhang J, Hu Y, Yang Y, Gou Z, Du T, Mao J, Gou M. A conformal hydrogel nanocomposite for local delivery of paclitaxel. J Biomater Sci Polym Ed. 2017; 28(1):107–118. [PubMed: 27765001]

70. Cook DJ, Nguyen C, Chun HN, I LL, Chiu AS, Machnicki M, Zarembinski TI, Carmichael ST. Hydrogel-delivered brain-derived neurotrophic factor promotes tissue repair and recovery after stroke. J Cereb Blood Flow Metab. 2017; 37(3):1030–1045. [PubMed: 27174996]

71. Tuladhar A, Morshead CM, Shoichet MS. Circumventing the blood-brain barrier: Local delivery of cyclosporin A stimulates stem cells in stroke-injured rat brain. J Control Release. 2015; 215:1–11. [PubMed: 26226344]

72. Wang Y, Cooke MJ, Sachewsky N, Morshead CM, Shoichet MS. Bioengineered sequential growth factor delivery stimulates brain tissue regeneration after stroke. J Control Release. 2013; 172(1):1– 11. [PubMed: 23933523]

73. Zhang L, Zhang F, Weng Z, Brown BN, Yan H, Ma XM, Vosler PS, Badylak SF, Dixon CE, Cui XT, Chen J. Effect of an inductive hydrogel composed of urinary bladder matrix upon functional recovery following traumatic brain injury. Tissue Eng Part A. 2013; 19(17-18):1909–18. [PubMed: 23596981]

74. Wu Y, Wang J, Shi Y, Pu H, Leak RK, Liou AK, Badylak SF, Liu Z, Zhang J, Chen J, Chen L. Implantation of Brain-derived Extracellular Matrix Enhances Neurological Recovery after Traumatic Brain Injury. Cell Transplant. 2016

## Statement of Significance

In situ gelation of ECM is essential for its retention within a tissue cavity. The brain is a unique environment with restricted access that necessitates image-guided delivery through a thin needle to access tissue cavities caused by stroke, as well as other conditions, such as traumatic brain injury or glioma resection. Knowledge about a brain tissue response to implanted hydrogels remains limited, especially in terms of long-term effects and potential impact on behavioral function. We here address the long-term retention of hydrogel within the brain environment, its impact on behavioral function, as well as its ability to reduce further tissue deformation caused by stroke. This study highlights considerable differences in the brain's long-term response to an ECM hydrogel compared to peripheral soft tissue. It underlines the importance of understanding the effect of the structural presence of a hydrogel within a cavity upon the host brain tissue and behavioral function. As demonstrated herein, ECM hydrogel can fill a cavity long-term to reduce further progression of the cavity, while potentially serving as a reservoir for local drug or cell delivery.
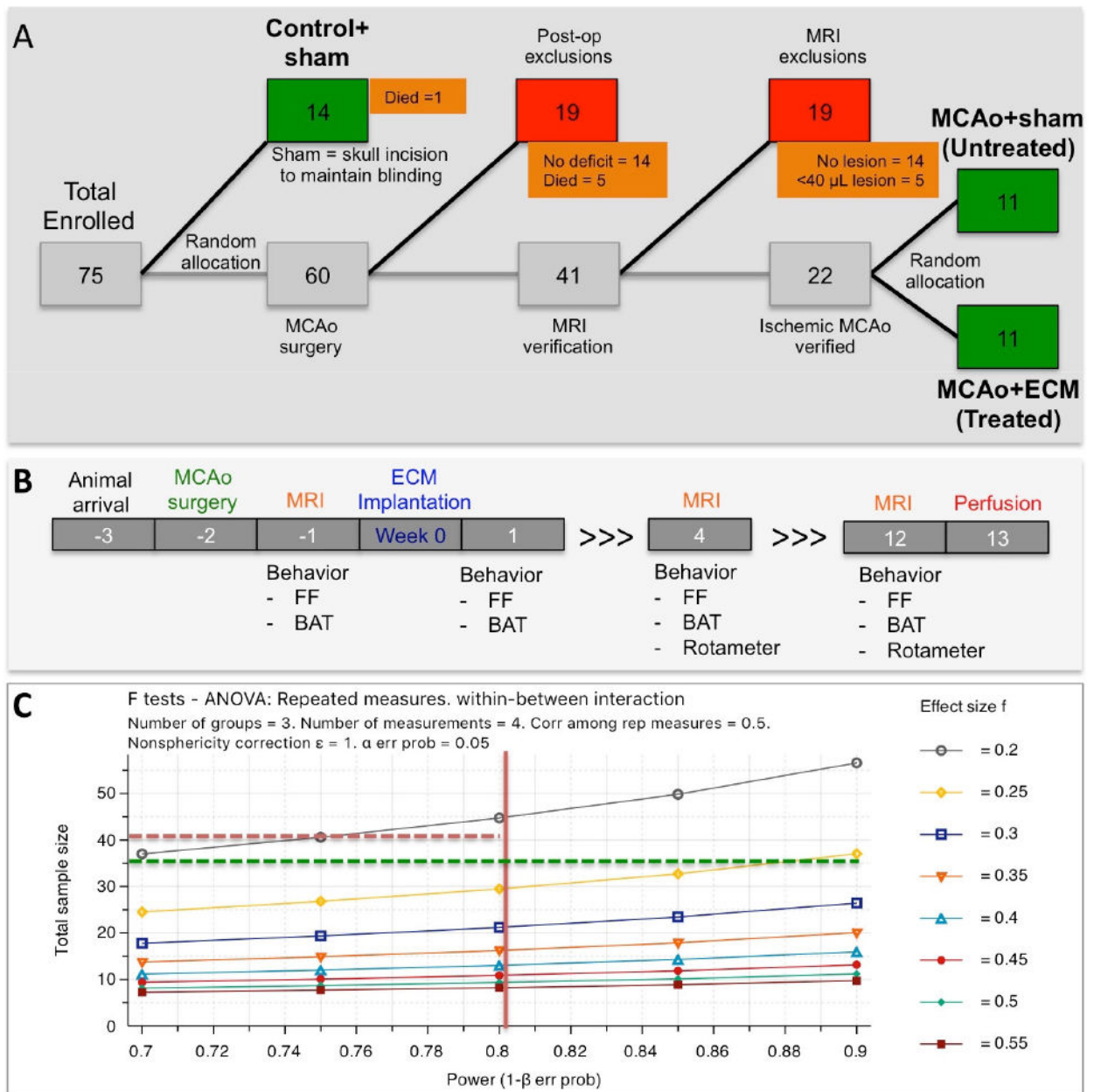
**Figure 1. Experimental Design**

**A** Diagrammatic representation of animals enrolled in the study charts the inclusion and exclusion of animals, as well as their random group allocation points. **B.** Overview of experimental time line with procedures performed on animals in relation to implantation of ECM hydrogel (week 0). **C.** A priori calculations to define a sufficient sample size as a function of statistical power (1-β) and effect size (f for ANOVA analyses). A power of 80% is considered sufficient to account for Type II errors, whereas a statistical significance of p<0.05 is considered a threshold for Type I errors. Considering these parameters, the 36 animals enrolled here will achieve sufficient power if a medium effect size of 0.25 is achieved.
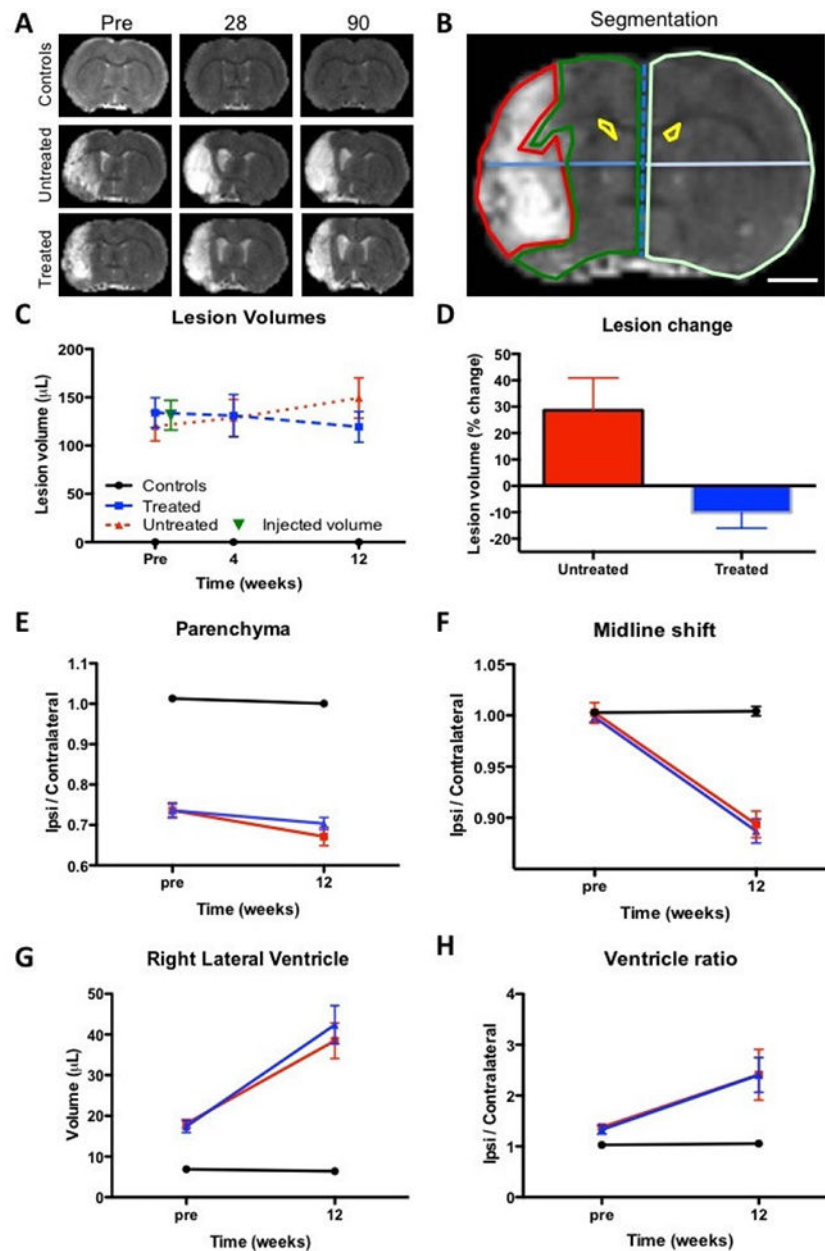
**Figure 2. Evolution of lesion volume and tissue deformation**

**A** T$_2$-weighted MR images of experimental groups over time reveal the hyperintense lesion cavity in animals with stroke damage. **B.** Measurement of lesion volume (red region-of-interest) based on the hyperintense T$_2$-weighted signal on MR images defined by mean signal of the contralateral hemisphere + 1 standard deviation (scale bar 2 mm). Ipsilateral (green) and contralateral (light green) parenchymal tissue, lateral ventricles (yellow) were also segmented on MR images. Midline shift (blue line) was calculated by a ratio between distance of the ipsilateral and contralateral hemisphere midpoints. **C.** Lesion volume was calculated for a baseline pre-implantation time point, as well as for 4 and 12 weeks post-implantation. **D.** To account for variations in lesion volume at baseline, % change between baseline and 12 weeks were calculated. **E.** A ratio of parenchymal volume revealed a

significant loss of parenchyma in stroke animals, which further declined a little over 12 weeks. **F.** A gradual shift of the midline was evident in both stroke groups, but was not impacted by ECM hydrogel implantation. **G.** An equivalent dramatic increase in ipsilateral lateral ventricle was evident in both stroke groups. **H.** The ratio between the ipsilateral and contralateral ventricle further reflect these gradual long-term changes in tissue structure after stroke. ECM hydrogel did not affect these tissue deformations.
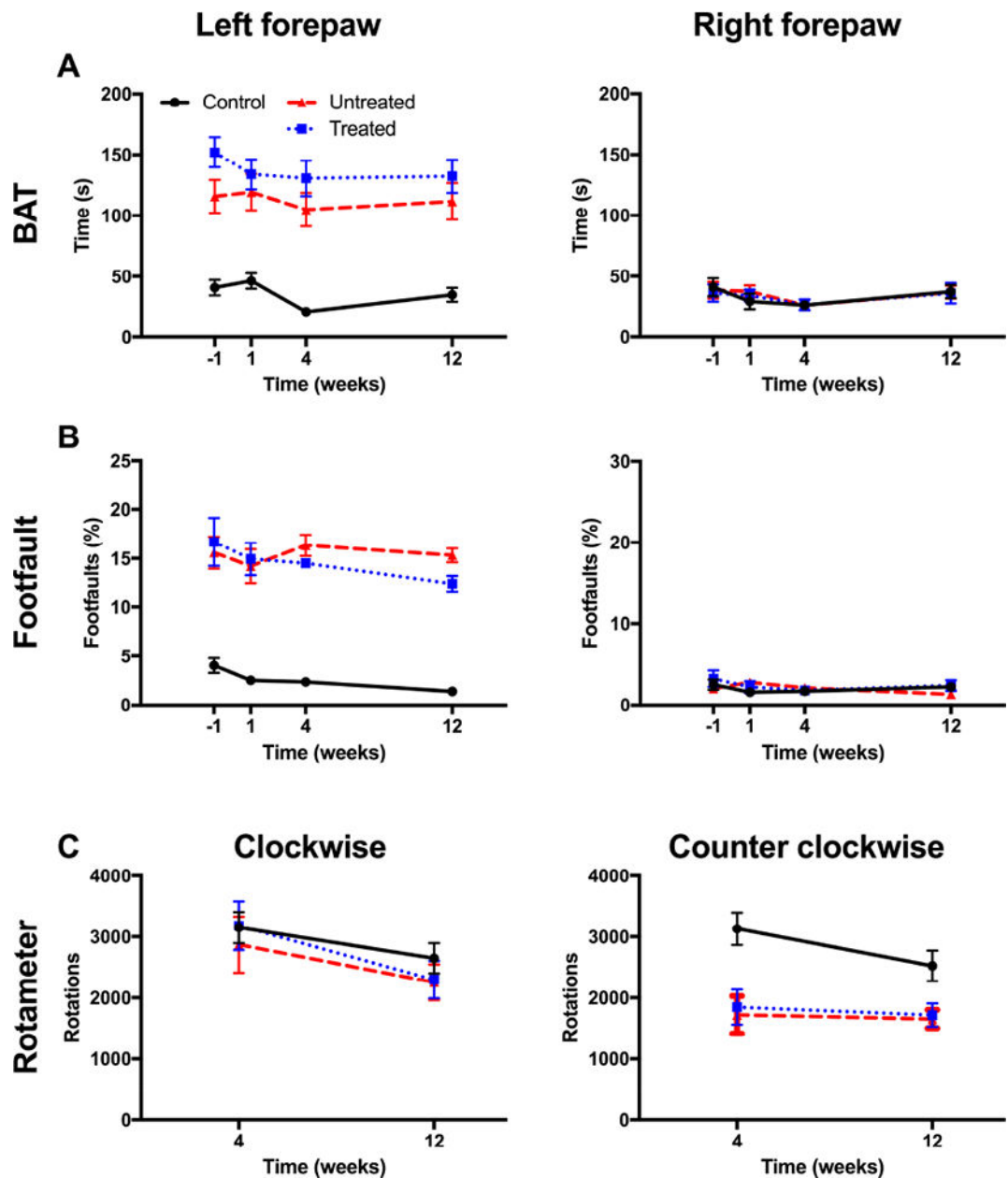
**Figure 3. Behavioral assessment**

**A** Bilateral asymmetry test (BAT) analyses revealed a significant sensorimotor bias in the left forepaw, but not in the right forepaw in untreated and treated animals. **B.** Treatment did not affect sensorimotor bias compared to untreated animals. The footfault test measured motor integration, which was significantly impaired in the left affected forepaw. Treated animals performed comparably to untreated animals on this task. **C.** Amphetamine-induced rotation bias on the rotameter reveals striatal integrity and dopamine responsiveness. Treated and untreated rats exhibited a comparable asymmetry in rotation.
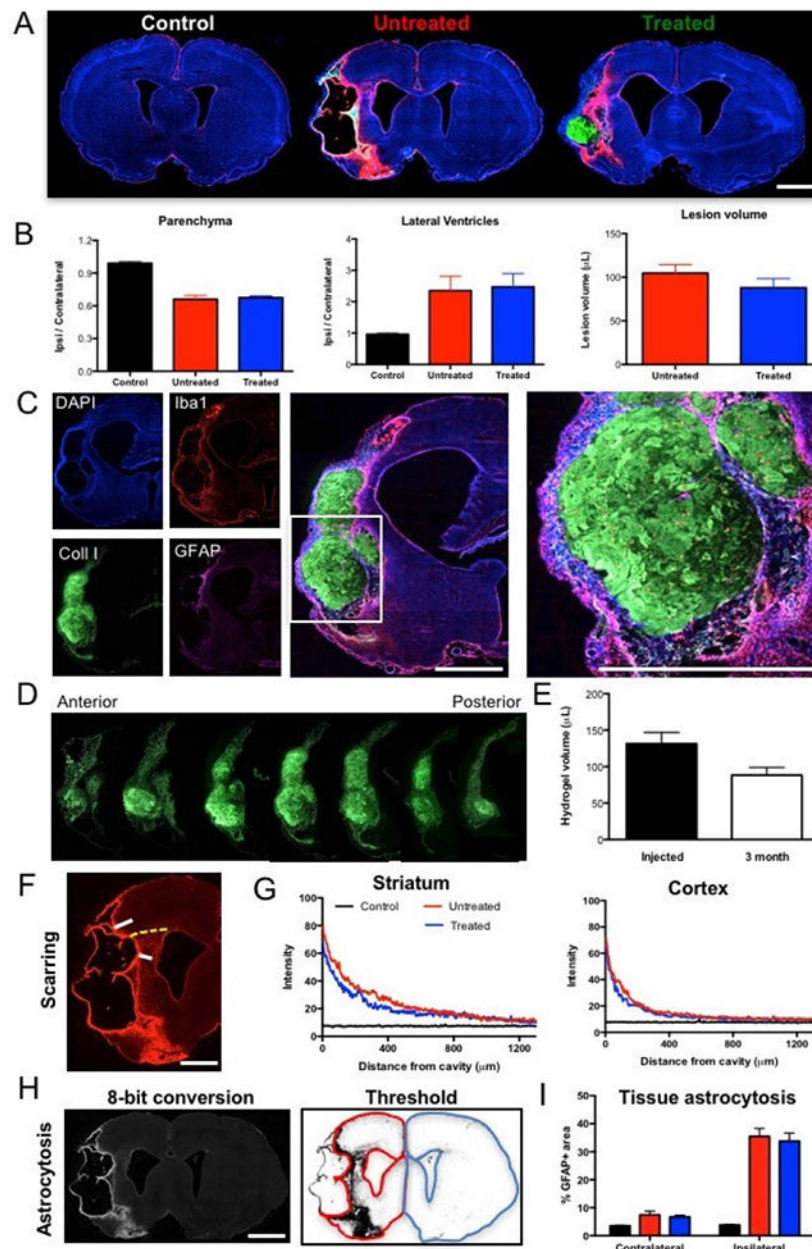
**Figure 4. ECM hydrogel retention and glial scarring**

**A** A histological comparison between controls, untreated and treated stroke animals reveals a major tissue loss in the ipsilateral hemisphere, as well as the presence of ECM hydrogel within the lesion cavity. **B.** A quantification of parenchymal volume in these 3 groups indicated a 33% tissue loss in animals with stroke, as well as a dramatic increase in ipsilateral ventricular volume. A treatment effect was evident on stroke lesion volume with a 19.8% decrease in cavity volume. **C.** ECM hydrogel was retained inside the lesion cavity in all treated animals as indicated by collagen I staining surrounded by host tissue. **D.** Along the anterior-posterior axis, ECM hydrogel was identifiable as a morphologically distinct entity aided by collagen I staining. **E.** A comparison between injection volume of ECM gel precursor and volume of hydrogel at 3 months revealed a decrease of 32%, but due to

individual variability this did not reach statistical significance. **F.** To evaluate the impact of ECM hydrogel on glial scarring at the tissue interface, whole brain slice images covering the lesion cavity along the anterior-posterior axis were acquired for all 3 groups to measure the level of astrocytic (GFAP) reactivity inside striatal and cortical tissue. **G**. A marked increase in GFAP staining was evident at the border of the lesion cavity that gradually decreased further inside the tissue. GFAP reactivity in the stroke-damaged striatum was higher than in the cortex. However, there was no significant difference between untreated and treated animals. **H.** Peri-infarct astrocytosis (i.e. the area occupied by reactive astrocytes) in the ipsilateral and contralateral parenchyma was measured by an 8-bit conversion of whole slice images to apply a threshold that created a binary map. **I.** This binary image afforded quantification of area occupied and provided a comparison of the 3 experimental groups to indicate that there was no significant difference between untreated and treated animals, although both had significantly more astrocytosis than normal controls. Scale bar 2 mm.
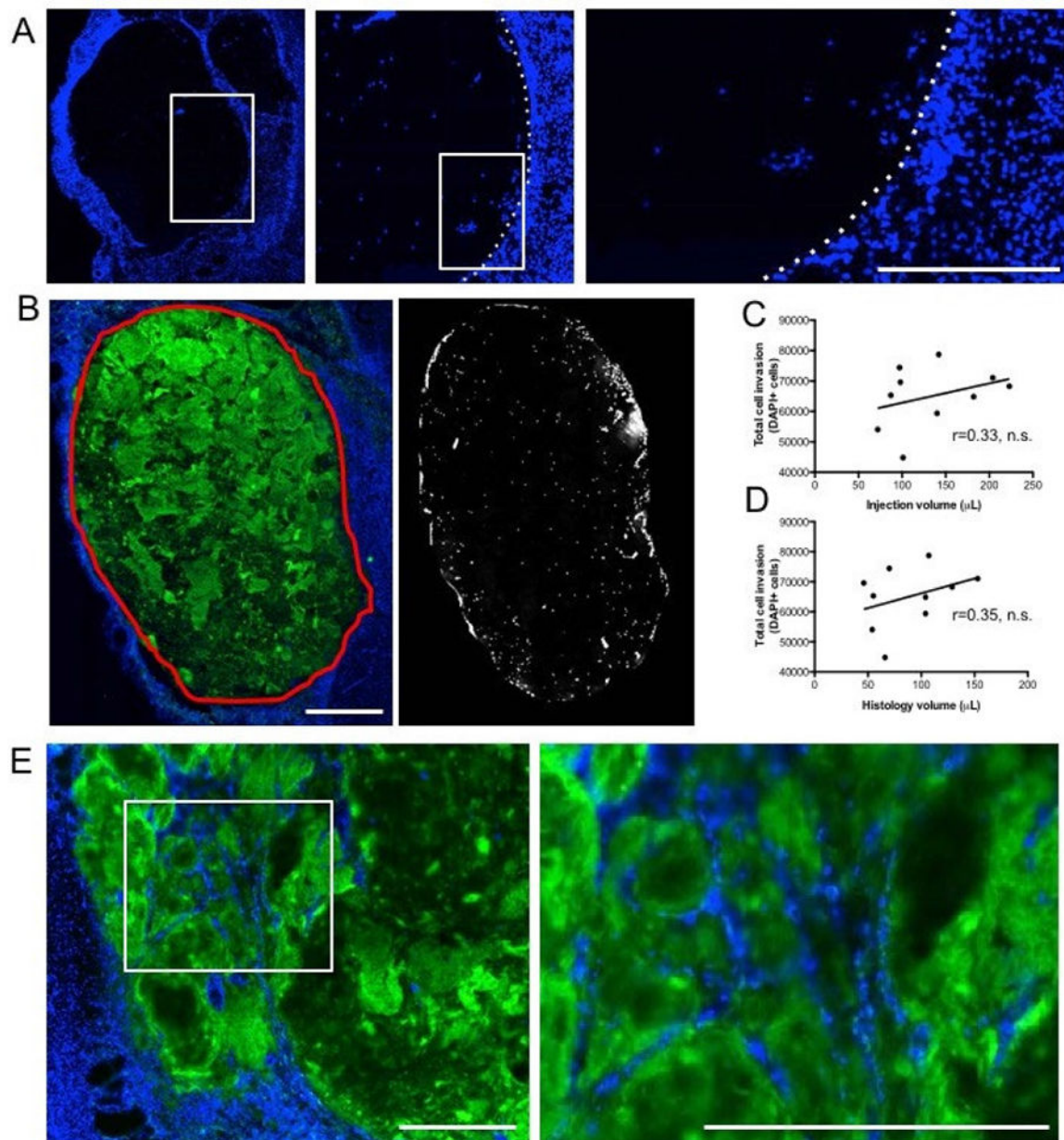
**Figure 5. Presence of host cells in ECM hydrogel**

**A** A sharp boundary of DAPI cells defined the interface between biomaterial and host brain with some cells being present within the ECM hydrogel. **B.** Using collagen I staining, a region-of-interest for the ECM hydrogel was defined and applied to the DAPI image to provide a quantification of the number of cells present within the hydrogel at 12 weeks post-implantation. A mean invasion of 65,050 cells with a range of 44,820-78,740 cells was measured. **C.** A non-significant (n.s.) correlation between injection volume of ECM or histological volume of ECM at 12 weeks indicates that the number of invading cells was not directly related to the volume of ECM injected into the brain. The regression line in the scatter plot reflects the steepness of the correlation between the two data sets. **D**. There was also no significant association between the degree of stroke damage (i.e. lesion volume) and

the number of invading cells, further highlighting that other factors play an important role in host cell invasion. **E.** Host cells that invaded and remained within the ECM hydrogel appear to be localized along topological grooves revealed by collagen I staining. Scale bars 100 μm.
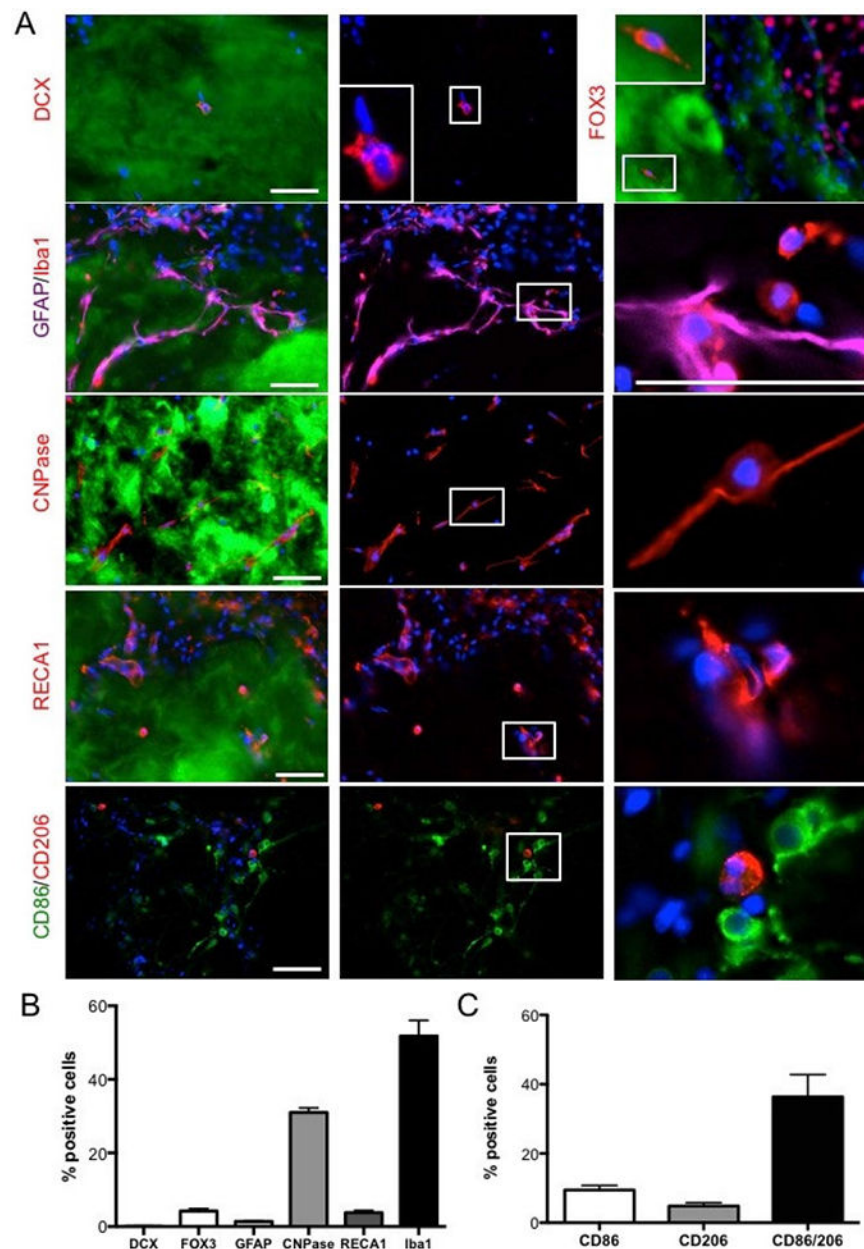
**Figure 6. Phenotypic characterization of cells in ECM hydrogel**

**A** Immunohistochemical characterization of individual cell phenotypes within the ECM hydrogel at different magnifications. **B.** A phenotypic analysis of cells present within the hydrogel were predominantly microglia (ionized calcium binding adapter molecule 1, Iba-1), as well as fewer (p<0.01) cells from the oligodendrocyte lineage (2′,3′-cyclic-nucleotide 3′-phosphodiesterase, CNPase). Significantly (p<0.001) fewer neurons (Fox3), neural progenitors (doublecortin, DCX), astrocytes (glial fibrillary acid protein, GFAP) or endothelial cells (rat endothelial cell antigen 1) were found. **C.** A comparison of monocyte polarization indicated that these mostly co-expressed M1 (CD86) and M2 (CD206) markers,

with significantly fewer cell expressing only CD86 (p<0.01) or CD206 (p<0.001). Scale bars 100 μm.

**Table 1**

List of antibodies used for immunohistochemistry.

| Antibody | Concentration | Company | Cat. Ref. | Clone |
|---|---|---|---|---|
| Collagen-I | 1:250 | Abcam | Ab34710 | Collagen I aa 1-1464 |
| Iba-1 | 1:300 | Abcam | Ab5076 | Iba1 aa 135-147 |
| GFAP | 1:3000 | Sigma | G3893 | G-A-5 |
| DCX | 1:150 | Abcam | Ab153668 | CAA0661′7.1 and AAT58219.1 |
| CNPase | 1:200 | Abcam | Ab6319 | 11-5B |
| Fox3 | 1:500 | Abcam | Ab104224 | 1B7 |
| RECA-1 | 1:100 | Abcam | Ab9774 | RECA-1 |
| CD86 | 1:200 | Abcam | Ab53004 | EP1159Y |
| CD206 | 1:200 | Santa Cruz | sc-34577 | C-20 |